Main Manuscript for

Load transfer between permanent and dynamic networks due to stress gradients in nonlinear viscoelastic hydrogels

Jikun Wang[1], Kunpeng Cui[2,5], Bangguo Zhu[1], Jian Ping Gong[2,3,4,*], Chung-Yuen Hui[1,3,*] and Alan T. Zehnder[1,*]

[1]Field of Theoretical & Applied Mechanics, Dept. of Mechanical & Aerospace Engineering, Cornell University, Ithaca, NY 14853, USA

[2]Institute for Chemical Reaction Design and Discovery (WPI-ICReDD), Hokkaido University, Japan

[3]Global Station for Soft Matter, GI-CoRE, Hokkaido University, Sapporo, Japan

[4]Faculty of Advanced Life Science, Hokkaido University, Japan

[5]Department of Polymer Science and Engineering, University of Science and Technology of China

*Corresponding author:

Jian Ping Gong[2,3,4,*], Chung-Yuen Hui[1,3,*] and Alan Zehnder[1,*]

Email: gong@sci.hokudai.ac.jp, ch45@cornell.edu, atz2@cornell.edu

Author Contributions: J. P.G., C. Y. H. and A. T. Z. designed research; J. W. and K. C. performed research; J. W., K. C. and B. Z. analyzed data; and J. W., K. C., B.Z, J. P.G., C. Y. H. and A. T. Z. wrote the paper.

Competing Interest Statement: The authors declare no competing interest

Keywords: dynamic bonds, chemical bonds, physical bonds, image correlation, viscoelasticity, crack

Abstract

Relaxation experiments are performed on single edge notch tension (SENT) and *T* shape specimens consisting of different variations of polyampholyte (PA) hydrogels. These specimens share a common feature of containing regions of high and low stress/strain. This feature enables us to probe the load transfer mechanisms between permanent and dynamic networks of different strengths. This load transfer mechanism is connected to viscoelastic behavior. PA gels are nonlinear viscoelastic, with time-dependent behavior controlled by the breaking and reforming of ionic bonds in the dynamic network. In contrast to the prediction of linear viscoelastic theory, the displacement and strain fields during stress relaxation are not fixed but change with time in a complex way depending on the strength of the dynamic bonds and the observation time window. These experimental results are explained by a nonlinear viscoelastic model. Additional physical insights are gained by appealing to the nonlinear rheology of dynamic bonds or stickers. Our result shows that load transfer between networks can be controlled by modifying the strength of dynamic bonds.

1. Introduction

The area of hydrogels has undergone great advances since the development of double network (DN) gels [1,2] which provides a path to toughen an otherwise brittle solid. However, because the networks in DN gels are chemically cross-linked, the damage to the sacrificial network due to overload cannot be recovered. This shortcoming motivated material chemists to fabricate gels with networks crosslinked by dynamic bonds [3–5]. These include dynamic covalent bond, hydrogen bond, ionic bond, metal-ligand coordination, host-guest interactions, hydrophobic interactions, and $\pi - \pi$ stacking [6–12]. Often, dynamic bonds serve as sacrificial bonds to dissipate energy, which is a key toughening mechanism. However, unlike DN gels, physical bonds in the dynamic networks can reform which leads to useful mechanical behavior such as self-healing and improved fatigue resistance [13–16].

Tough and self-healing hydrogels usually have two distinct dynamic modes of polymer networks, where one is crosslinked by the dynamic bonds, and another is crosslinked by the covalent bonds and/or entanglements. Load transfer between two networks is important to predict the failure near stress concentrators such as the tip of a preexisting crack. For example, in a gel consisting of both permanent and dynamic networks, crack growth cannot occur until both networks fail. This failure depends on the load transfer mechanics between the permanent and the dynamic networks. In many systems, the dynamic network consists of sacrificial bonds which break to dissipate energy

and to protect chains in the permanent network [17,18]. This load transfer problem is of great importance to the development of tough gels, yet it is poorly understood.

Depending on the time observation window, soft materials with dynamic networks can exhibit strong or weak viscoelastic behavior. At present, our understanding of viscoelasticity is still rather incomplete. Many analyses and physical interpretations rely on linear viscoelastic theory, which is well developed but limited to small strains. For example, the storage and loss moduli of soft materials are typically determined by rheology testing at strains on the order of 1%. In applications, strains in soft materials can easily exceed several hundred percent. More importantly, linear viscoelasticity assumes that relaxation times) are material properties, independent of stress and strain history. However, as noted by [6,19–21], the bond breaking and healing kinetics in most dynamic networks are sensitive to the force or stretch acting on the chains. This means that relaxation times are not material properties but depend on the history of stress or strain. This nonlinear effect is expected to play a key role in the load transfer between the two networks in tough, soft materials.

In recent years, there has been a surge of interest using discrete and quasi-continuum approaches to learn the effect of bond breakage and formation on the mechanical response and viscoelastic behavior of polymer networks [22–25]. In this work we shed light on this load transfer problem and how it depends on dynamic bond (sticker) strength using polyampholyte (PA) gels with two types of stickers developed by Sun et al. [26]. We study four PA gels. Specifically, for each type of stickers, we prepare gels with or without a chemical cross-linker N, N′-methylenebisacrylamide (MBAA). We call these *c-PA* and *p-PA gels*, respectively. The dynamic bond of the 1st type is formed by p-styrenesulphonate (NaSS) and N-dimethylaminoethylacrylate (DMAEA-Q). The softening temperature of this gel is 17.3 ℃ which is below room temperature. The 2nd type of dynamic bond is formed by NaSS and 3-(methacryloylamino) propyl-trimethylammonium chloride (MPTC), with softening temperature at 48.2 ℃. In our experimental observation window, the modulus and viscoelasticity of the 2nd is much greater than the first, so we call the first dynamic bonds *weak* stickers and the second are called *strong* stickers. In the following, gels with strong/weak stickers will be labeled by $c\text{-}PA_{strong/weak}$ and $p\text{-}PA_{strong.weak}$ respectively.

2. Materials and Methods

Materials: $c\text{-}PA_{weak}$ and $p\text{-}PA_{weak}$ gels are made from p-styrenesulphonate (NaSS) and N-dimethylaminoethylacrylate (DMAEA-Q), with and without MBAA (Wako Pure Chemical

Industries Ltd., Japan) as crosslinker. *c-PA$_{strong}$* and *p-PA$_{strong}$* are made from NaSS and 3-(methacryloylamino) propyl-trimethylammonium chloride (MPTC) with and without MBAA.

Synthesis: For the gels with weak stickers, P(Nass-co-DMAEA-Q) gels, the concentration of monomers (NaSS and DMAEA-Q) is 2.5 M and the molar ratio is NaSS: DMAEA-Q = 0.516 : 0.484. The concentration of initiator α-keto is 0.1 mol% with respect to monomer concentration. The concentrations of MBAA are 0, 0.3 and 0.5 mol%, respectively. For the gels with strong stickers, the concentration of monomers (NaSS and MPTC) is 2.1 M and the molar ratio is NaSS : MPTC = 0.517 : 0.483. The concentration of α-keto is 0.25 mol%. The concentrations of MBAA are 0 and 0.3 mol% respectively. In both gels, the precursor solution containing was deoxidized in an Argon glove box and then injected and sealed into a mold made by glass plates and silicone rubber spacer (120 mm × 12 mm × 2.2 mm. The solution was polymerized under UV irradiation for 11 hours. After polymerization, the as-prepared gel was soaked in deionized water for one week to remove counter-ions and to reach equilibrium. The deionized water was changed every day.

Tension test: We use a load cell (Interface, SMT1-100N) to record the change of force or nominal stress σ_N and digital image correlation (DIC) to monitor the change of strain field for the whole specimen during relaxation [27]. Details of the DIC measurements are given in section S1 in the supporting information. All tests are performed in deionized water to prevent the gels from drying.

3. Results and Discussion

The network of *c-PA$_{strong}$* consists of a dynamic network crosslinked by ionic bonds and a permanent network crosslinked by chemical crosslinker and reinforced by trapped physical entanglement. Figure 1a shows the dynamic spectra of this gel, which exhibits strong frequency-dependent moduli in an extremely wide frequency range from 10^{-5} to 10^{4} /s. This wide frequency viscoelasticity is attributed to high density of ionic bonds. For frequencies smaller than 10^{-5} /s, the gel shows a plateau modulus, due to the permanent confinement by the chemical crosslinkers and physical entanglements.

The *p-PA$_{strong}$* gel consists of two dynamic networks crosslinked by dynamic bond and physical entanglement, respectively. This gel shows similar dynamic behavior as *c-PA$_{strong}$* gel, except that the plateau modulus is from physical entanglement and in theory has no long-time modulus. However, the motion of the whole chain is significantly delayed by the stickers. We do not see the flow of this gel even for a timescale up to 10^{7} s (Fig. 1b). This is due to the slowing down of Rouse modes (sticky Rouse) caused by the strong stickers [30]. Also, the distribution in the strength of

ionic bonds, owing to the 100 nm-scale phase separation structure [31], could be another reason for the wide frequency viscoelasticity.

The other two gels with weak stickers are denoted as *c-PA*$_{weak}$ and *p-PA*$_{weak}$ gels, respectively (Figures 1c and 1d). These two gels have a weaker sticker and thus the sticky Rouse region shifts to high frequency region compared to the gels with strong stickers. We also do not see flow of *p-PA*$_{weak}$ gel for a timescale up to 10^4 s (Fig. 1d). In the following mechanical tests, we fixed our strain rate at 0.1 /s, at which the gels with strong stickers are strongly viscoelastic, whereas the gels with weak stickers are weakly viscoelastic.

In addition, we can see that for *c-PA*$_{strong}$ and *p-PA*$_{strong}$, both G' and G" are bending towards asymptotic values in the limit of high strains, while for *c-PA*$_{weak}$ and *p-PA*$_{weak}$, both moduli are approximately linear in strain rate. This is because the physical PA gels with strong bonds have a long sticker lifetime. In the limit of high strain rates (or frequencies) in our rheological experiments, the dynamic bonds do not have time to break. Therefore, the moduli tend towards a constant value at high frequencies. The PA gels with weak bonds have a short lifetime. Even in the high frequency regime in our experiments, they still can dissociate. Therefore, the moduli increase with frequency.

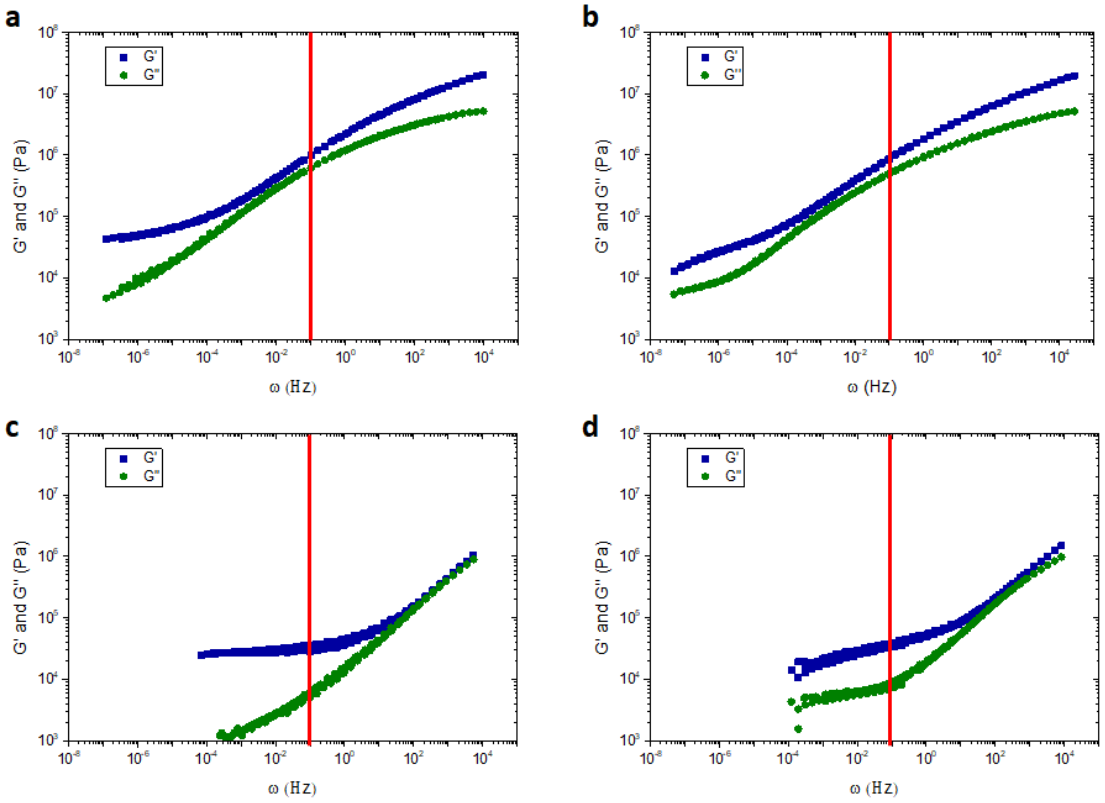

Figure 1: Dynamic mechanical spectra of four gels used in this work: (a) *c-PA*$_{strong}$, (b) *p-PA*$_{strong}$, (c) *c-PA*$_{weak}$, and (d) *p-PA*$_{weak}$. Reference temperature: 25 °C. *c-PA*$_{strong}$ and *c-PA*$_{weak}$ gels consist of a dynamic network crosslinked by ionic bonds and a permanent network crosslinked by chemical crosslinker and physical entanglement. *p-PA*$_{strong}$ and *p-PA*$_{weak}$ consist of two dynamic networks crosslinked by ionic bonds and physical entanglement, respectively. Red lines correspond to the strain rate of 0.1/s used in the following tensile tests, where *c-PA*$_{strong}$ and *p-PA*$_{strong}$ gels are strongly viscoelastic, while *c-PA*$_{weak}$ and *p-PA*$_{weak}$ gels are weakly viscoelastic, owing to the different strengths of stickers.

3.1 Nonlinear effect of c-PA$_{strong}$ *gel having a permanent network and a dynamic network.*

SENT specimens loaded in Mode I:

In a *linear* viscoelastic solid, the relaxation function is independent of the stress/strain history, hence the speed of stress relaxation in a relaxation test is spatially uniform in the cracked specimen, despite the high stress/strain concentration near the crack tip [27]. However, for nonlinear viscoelastic solids, the relaxation function depends on the strain or stress level. If the strain field is non-uniform, the speed of stress relaxation can vary greatly in different parts of the specimen. This phenomenon is expected to be most significant near the crack tip, where the strain gradient is very large. To observe this behavior, we perform a relaxation test using the SENT specimen (Fig. 2a). Thicknesses of specimens range from 1.9 mm to 2.1 mm. In-plane dimension is 20 mm $\left(L_0\right)$ × 10 mm $\left(W_0\right)$ with a 2 mm crack at the middle of one edge. We stretch the specimen (with initial length L_0) to a nominal stretch ratio of $\lambda_N = L/L_0 = 1.5$ with a fast stretch rate of 0.1/s and then hold it at the deformed length $L = 1.5L_0$ for half an hour. The strain distribution is measured using Digital Image Correlation (DIC) (Section S1).

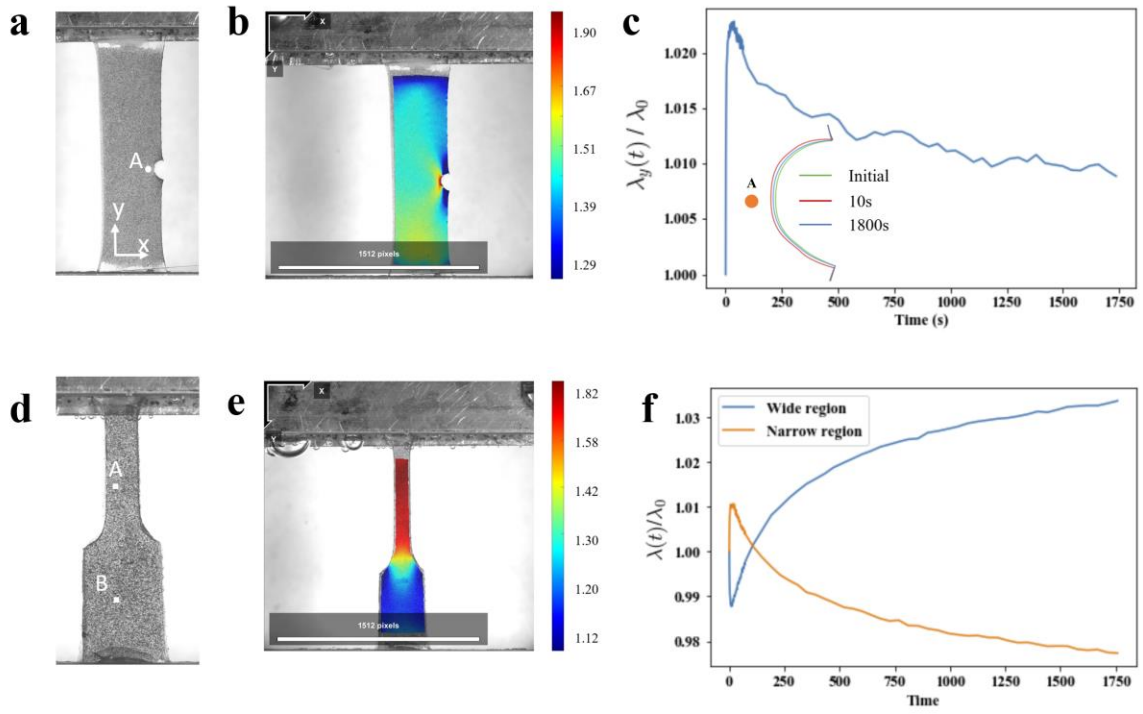

Figure 2: Nonlinear relaxation of *c-PA*$_{strong}$ gel. (a) SENT specimen. (b) Strain distribution in SENT specimen after loading. (c) Time evolution of stretch at *A* (see Fig. 1a) and COD (insert) in SENT specimens in relaxation tests. (d) *T*-shape specimen. (e) Strain distribution in *T*-shape specimen after loading. (f) Time evolution of stretch at narrow and wide sections in *T*-shape specimen. In (c) and (f), t = 0 is the time when relaxation starts, specifically, the nominal stretches reach their maximum values. λ_0 is the local stretch in the y direction at t = 0.

Figures 2a-c show the crack shape and the evolution of the stretch ratio in the direction normal to the crack line λ_y at the point *A* which is 1 mm directly ahead of the crack tip for *c-PA*$_{strong}$ gel specimen. This gel shows a result at odds with linear viscoelasticity which predicts that the displacement and strain field during relaxation should not change with time. Specifically, despite the displacement being fixed at the grips, $\lambda_y(t)$ increases rapidly for ten seconds during relaxation and then *closes* slowly in the following half hour. Also, the crack opening displacement (COD) shows the same behavior (see insert in Fig. 2c) – it increases rapidly first, and then decreases slowly over the following half hour.

T-shape specimen Tests (T test):

The above relaxation experiments show that the strain near the crack tip for the *c-PA*$_{strong}$ gel first increases and then decreases during stress relaxation. The crack geometry makes this problem

very difficult to analyze. However, the key features of this phenomenon can be explained by the hypothesis that the breaking kinetics of dynamic bonds are strain dependent: the relaxation time is *not a material property* but is sensitive to the strain history acting on the network. If this hypothesis is correct, then we should be able to see the same phenomenon in the *T*-shape specimen in Fig. 2d. The *T*-shape specimen has the same thickness and length as the SENT specimen, the width of the wide section (WS) is 10 mm, two times wider than the narrow section (NS). The edge of the intersection between the sections is slightly rounded to reduce stress concentration. In this specimen, each section of the specimen has approximately uniform, but different strain, with the NS bearing higher strain. This means that the NS should relax faster and hence be more compliant. Since the same tension force is acting on both sections, the strain in the NS must increase. This increase in strain in the NS must be compensated by an equal decrease in strain in the WS since the total displacement is fixed during relaxation.

The common feature between the *T* test and the crack test is the presence of stress/strain gradient. In SENT specimen, the strain near the crack tip is higher than the strain away from the crack tip; in the *T* test, the strain in the NS is higher than the strain in the WS. The strain field distribution measured by DIC in both experiments and for this gel at the beginning of relaxation is shown in Fig. 2b and 2e.

Based on this similarity, we use the *T* test to help us understand what happens to the strain and stress fields near the crack tip during relaxation. Note that it is much easier to perform theoretical and numerical analysis for the *T* tests. By analyzing the stress field of *T*-shape specimen during relaxation, we gain insight into how the stress/strain field changes near the crack tip during relaxation and how this nonlinear viscoelastic effect would affect fracture.

With this motivation, we perform relaxation tests on the *T*-shaped specimen. Specifically, specimen is stretched to a nominal stretch $\lambda_N = 1.5$ at a constant stretch rate of 0.1/s; then held for a half hour. The strain history is measured using DIC. Near the boundary of the two sections, the strains are non-uniform. Our DIC measurements indicate that this non-uniformity decays rather rapidly so that the strain away in each section, away from the boundary, is approximately uniform. The stretch history of *c*-PA_{strong} gel after loading is shown in Fig. 2f. Here $\lambda(t)$ denotes the stretch ratio along the loading direction at point A (NS) or B (WS), and λ_0 denotes the stretch at point A or B when relaxation starts.

The result in Fig. 2f is consistent with that in Fig. 2c. The strain in the NS of the *T* specimen first increases rapidly, reaches a maximum, then decreases slowly while the WS behaves oppositely.

The physics behind this difference can be explained as follows: the gel consists of a permanent network and a dynamic network, where the permanent network has a long-time modulus while the dynamic network does not. The existence of a long-time modulus means that there is a finite relaxation time where the gel can reach its relaxed state. In this fully relaxed state, the healed dynamic bonds do not carry any load. Even though the NS relaxes faster, eventually both sections reach their fully relaxed state, at this time the deformation is governed entirely by the hyper-elasticity of the permanent network. In a hyper-elastic solid, the strain distribution in a displacement-controlled test is independent of the modulus, hence the NS section must shrink from its maximum value and the strain in WS must increase to compensate.

Theoretical prediction of relaxation process in *T*-shaped specimen and comparison with experiments:

We further support the physical reasoning above using our constitutive model to simulate the relaxation behavior of the *T*-shaped specimen in Fig. 2f. Details of model and simulation are given in SI Appendix section S2-S4. Figure 3 compares the simulation results with experiments for the *c*-PA_{strong} gel. Simulations are solid lines and experimental data are symbols (dots).

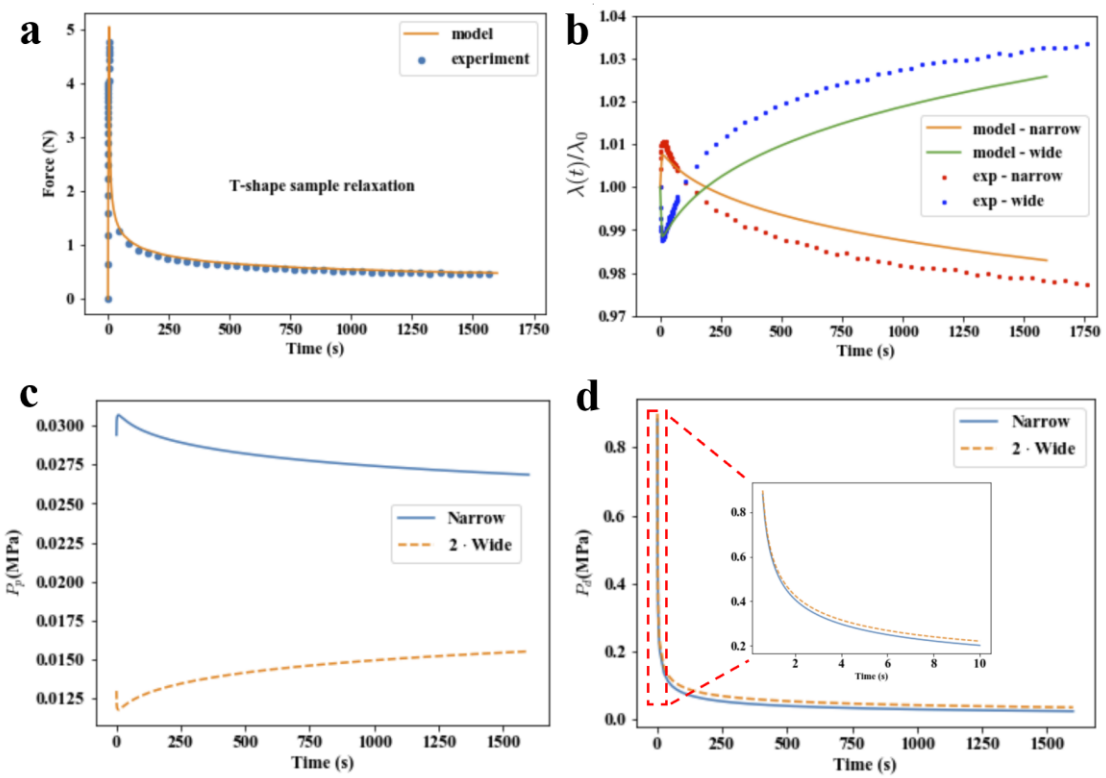

Figure 3: Load transfer between permanent and dynamic networks. (a) Measured force versus time curve for the *T*-shape specimen (b) Measured strain history (using DIC, symbols) versus simulated strain history (solid lines) during relaxation for *c-PA*$_{strong}$ gel. Nominal stress history of the *T*-shape *c-PA*$_{strong}$ gel during relaxation (t > 5s) for (c) permanent network, (d) dynamic network.

Let us denote the nominal stress in each section by *P*. In our constitutive model, we can *separately* calculate the nominal stress acting on the permanent $\left(P_p\right)$ and the dynamic network $\left(P_d = P - P_p\right)$ in the *c-PA*$_{strong}$ gel. These stresses are plotted in Fig. 3c and 3d for $t > T = 5s$ (when relaxation starts). Fig. 3c shows the time evolution of the nominal stress in the *permanent* network in the narrow and wide section, and Fig. 3d shows the stress evolution in the dynamic network. These curves are consistent with the chemical structure and tension test data of *c-PA*$_{strong}$ gel. In this gel, the permanent crosslink density is 0.3 mol% with respect to the monomer density, which is determined by the chemical crosslinker density, and the dynamic crosslink density is in the scale of 50 mol% with respect to monomer density, because one cationic and one anionic monomer can form one dynamic crosslink. As a result, in the T-shape sample test (Fig. 3a), the stress after 1500 s is less than 10% of the stress at the beginning, which is caused by the relaxation of stress in dynamic network. In our chemical PA model, this stress distribution is captured. As shown in Fig. 3c-d. at the beginning of relaxation, the stress in the dynamic network is 20 times higher than the stress in the permanent network; the stress in the two networks reaches the same level after 1500 s relaxation. For different gel systems, the stress level in the permanent and dynamic network may be different, according to their chemical components and concentration. In this work, we study only hydrogels with a high density of dynamic bonds. Note that most tough and self-healing hydrogels have a high density of dynamic bonds.[2,28,29]

Note that, despite *P decreasing* with time in the relaxation test, the stress acting on the permanent network (NS) *increases* during the first *10* sec, reaches a peak, then decreases to a steady value governed by the elasticity of the permanent network. The opposite is true in the wide section, as demanded by force balance. Fig. 3d shows that the stress in the *dynamic* network in the NS decays faster than the WS. At long times, the stress in both section decays to zero, indicating that the healed physical bonds no longer carry load, as predicted by our constitutive model.

The results in Fig. 3 validate our hypothesis; in addition, they indicate that our constitutive model captures the relaxation behavior of this gel system. To put these results in the context of our model,

we note that the relaxation function in our theory (see eqn. S4c) is dependent on the strain level. Since $P_{ns} = 2P_{ws}$ in our *T* specimens, the strain in the narrow section is higher, resulting in faster *stress* relaxation. However, the total force acting on each section is identical. To maintain force balance, the narrow section needs to be elongated to compensate for the faster decrease of the nominal stress, as shown in Fig. 3b. This explains the *increase* in strain acting on NS of the *c-PA*$_{strong}$ gel during the first 10 s (despite the decrease in total stress during this time).

At the beginning of relaxation, the force on the permanent network in the specimen is much smaller than the force on the dynamic network, so stress relaxation is dominated by the physical network (see Fig. 3c and 3d). Recall that the strain in the narrow section must elongate to maintain force balance, this elongation stretches the permanent network in the narrow section and increases P_p. After the first 10 seconds, the force on the dynamic network is roughly the same as the force on the permanent network, and it relaxes much *slower*. This is the reason the strain in the narrow region keeps decreasing for such a long time after the first 10 seconds. In this period, the interaction between the permanent network and the dynamic network dominates the relaxation process. In our model, the force on the dynamic network will eventually vanish at sufficiently long times and the force on the permanent network is governed by hyper-elasticity.

3.2. Nonlinear effect of p-PA$_{strong}$ *gel having an entangled network and a dynamic network.*

We performed the same measurements on the SENT and T-shape specimens of *p-PA*$_{strong}$ gel having an entangled network and a dynamic network. Strikingly, this gel shows a similar behavior as the *c-PA*$_{strong}$ gel, even though it has no chemical crosslinks. That is, during relaxation, the COD at first opens rapidly for one minute, and after that, the crack *closes* slowly in the following half hour (Fig. 4a, insert). $\lambda_y(t)$ at *A* also shows the same behavior as *c-PA*$_{strong}$ gel – it increases rapidly first, and then decreases slowly in the following half hour. Similarly, in the *T* specimens, the strain in the NS first increases rapidly, reaches a maximum, then decreases slowly while the WS behaves oppositely.

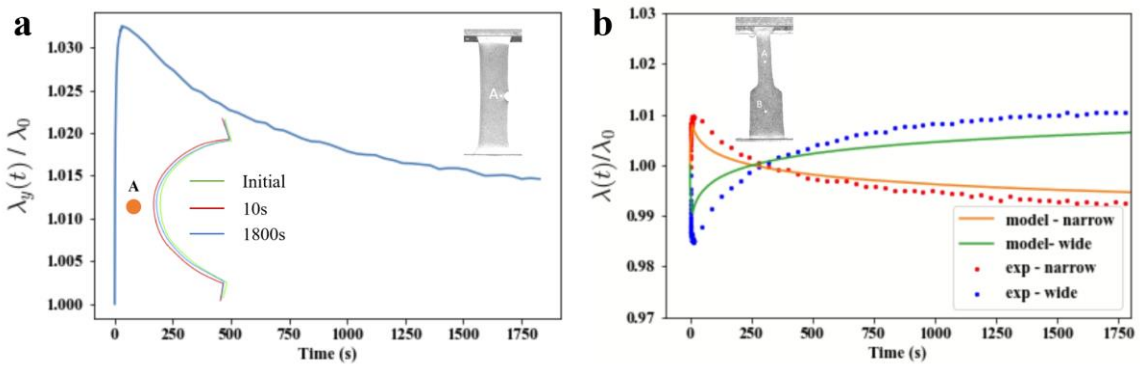

Figure 4: Nonlinear effect of *p-PA*$_{strong}$ gel. (a) Time evolution of stretch at *A* and COD (insert) in SENT specimens (insert) in relaxation tests. (b) Measured strain history versus simulated strain history during relaxation in *T*-shape specimen (insert) for *p-PA*$_{strong}$ gel. λ_0 is the local stretch in y direction at measured points at t = 0.

The question is why does the *p-PA*$_{strong}$ gel behave in the same way as the *c-PA*$_{strong}$ gel despite having no longtime modulus? The explanation is that *p-PA*$_{strong}$ gel has a very long relaxation time of topological entanglements between the chains. This relaxation time, called the sticky-reptation time, is controlled by the sticker lifetime and sticker density [30]. The strong sticker results in a very long sticky-reptation time so the topological entanglements of *p-PA*$_{strong}$ gel behaves like permanent crosslinks in the observation time window (~2000 s), as shown by Figure 2c. This suggests that the observed nonlinear behavior is general in soft materials with dual dynamic networks, provided that one network is dynamic and the other is "permanent" in the experimental observation window.

3.3 Effect of Sticker Strength

We next explore the role of sticker strength by performing the same relaxation test on the two gels with weak stickers. The *c-PA*$_{weak}$ gel in both SENT and *T*-shaped specimens behaves in a similar way as the *c-PA*$_{strong}$ and *p-PA*$_{strong}$ gels, albeit at a much weaker level (Fig. 5). The small increase in stretch at short times is attributed to the weak strength of stickers which reduces the elasticity of the network due to the accelerated breaking of dynamic bonds.

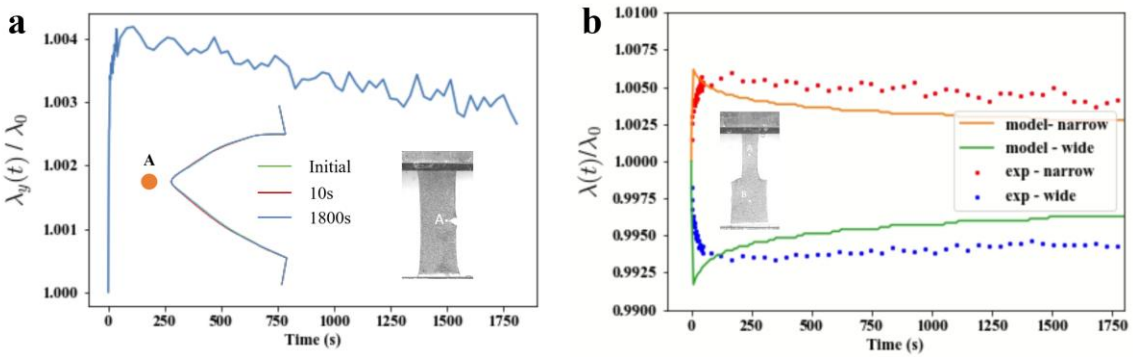

Figure 5: Nonlinear effect of *c-PA*$_{weak}$ gel. (a) Time evolution of stretch at *A* and COD (insert) in SENT specimens (insert) in relaxation tests. (b) Measured strain history versus simulated strain history during relaxation in *T*-shape specimen (insert) for *c-PA*$_{weak}$ gel. λ_0 is the local stretch in y direction at measured points at t = 0.

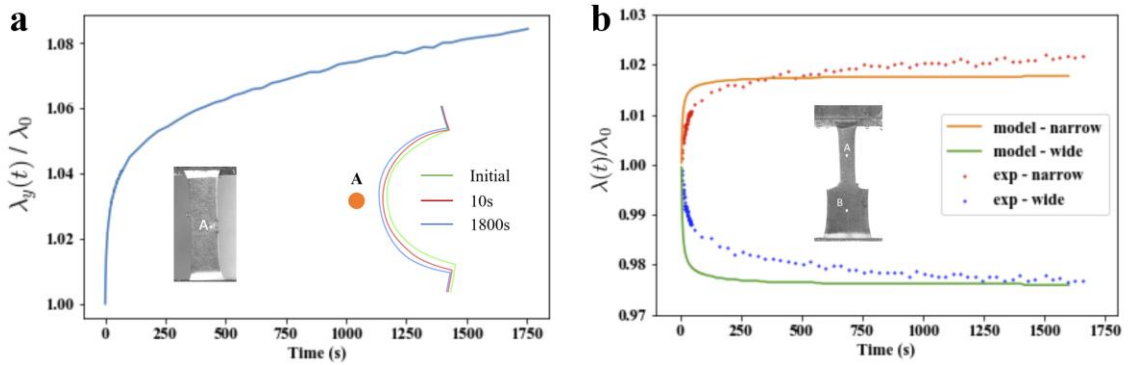

Figure 6: Nonlinear effect of *p-PA*$_{weak}$ gel. (a) Time evolution of stretch at *A* and COD (insert) in SENT specimens (insert) in relaxation tests. (b) Measured strain history versus simulated strain history during relaxation in T-shape specimen (insert) for *p-PA*$_{weak}$ gel. λ_0 is the local stretch in y direction at measured points at t = 0.

However, the *p-PA*$_{weak}$ gel exhibits a different behavior from the above three gels (Fig. 6). Specifically, during relaxation, COD opens rapidly in the first 10 seconds and then continues to *open* slowly in the following half hour. $\lambda_y(t)$ also increases rapidly first, and then *increases* slowly. Similarly, the strain in the NS in the *T* test continued to *increase* with time, eventually reaching a plateau when the stress relaxes to zero, whereas the WS behaves oppositely. This supports our hypothesis that, for weak stickers, the elasticity due to physical entanglement under *large* strain or stress is negligible, making it possible to observe relaxation to a fluid-like state, although from *small strain* dynamic spectrum the gel stays in elastic region in the experimental

observation window. We can also explain this by appealing to physically based rheology models (see discussion).

4. Summary and Discussion

We synthesized four PA gels with and without chemical crosslinks and with different sticker strengths. We carried out relaxation tests on *SENT* and *T* shaped specimens to study the effect of nonlinear viscoelasticity on the deformation fields. For *p-PA*$_{weak}$ gel with weak stickers, the stress near the crack tip drops faster than elsewhere due to the rapid breaking of the dynamic network; this causes the COD and strains near the crack tip to increase with time, while the strain away from the crack tip decreases with time. This further accelerates the breaking of the dynamic network near the crack tip. Since the grips are fixed, the COD for very long time will eventually reaches a steady state while the stress everywhere vanishes. We observe similar results for the *T*-shape *p-PA*$_{weak}$ specimen. This is not the case for physical gels with strong stickers, within the time windows of our experiments, these gels behave as if they are permanently crosslinked.

For chemical gels with strong stickers, the strain, and the COD near the crack tip during relaxation first increase, reach a maximum, then decrease to a steady value. During this period of rapid relaxation, the dynamic network unloads rapidly and the additional strain is transferred to the permanent network. At some point in time, the strain in the *permanent network* near the crack tip reaches its *maximum*. If the imposed nominal stretch on the specimen is large enough, it is possible to fail the permanent network during this stage *even while the stress is relaxing.* This load transfer mechanism suggests the possibility of *delayed fracture under stress relaxation*. After this period, if the crack does not propagate, then the chemical network near the crack tip will stretch less (the COD will decrease) and the crack may never propagate. Eventually, the dynamic network is fully relaxed everywhere, and all the load is born by the permanent network.

Simulations are carried out using a nonlinear viscoelastic constitutive model to compute the deformation and stress in the T-shaped specimens. We found reasonable agreement between experiments and theory for all four gel specimens.

Our experiments can also be understood by appealing to rheology models for associated polymers [30]. Let us return to the longtime behavior of the *p-PAweak* gel where the entangled network relaxes to its fluid-like state within observation time. According to Zhang et al.[30], this relaxation is governed by the sticky-reptation time $\tau_{rep} = \tau_s M^3 M_e^{-1} M_s^{-2}$,where M and M_e are the

molecular mass of a whole chain and an entangled strand, respectively and M_s is the average molecular mass between stickers. This equation for τ_{rep} shows that the entanglement effect is controlled by the sticker lifetime τ_s and sticker density M/M_s. Therefore, it is reasonable to conclude that physical PA gels such as *p-PAweak* gel with weak ionic interaction will act like a fluid at long times while the *p-PAstrong* gel will behave like a solid when τ_{rep} is larger than the observation time. This is supported by our results in Fig. 3-6. Likewise, the strength of stickers can also affect the behavior of chemical crosslinked gels. For example, if the stickers are weak, e.g., *c-PAweak* gel, the effect shown in Fig. 2c or 2f is much weaker, as shown in Fig. 5a and 5b. Specifically, the peak and decrease in Fig. 5a and 5b due to change of strains are barely perceptible since most of the stress is borne by the permanent network. Finally, we emphasize that occurrence of load transfer between the permanent/entangled and dynamic networks cannot take place without nonlinear viscoelasticity, that is, the sticker lifetime decreases with increasing strain. Specifically, the storage modulus versus frequency curve will shift to the right (higher frequency) as the strain increases. The net effect of this shift is changing the relaxation behavior within observation window.

Finally, we address whether poroelastic flow can be partially responsible for our observations. First, we note that the behavior for both the crack and T shape samples are very similar: rapid changes of the stretch ratio occurring in roughly 10 seconds – this is much faster than the diffusion time scale. Therefore, the effect of water flow will be much more prominent in the crack sample which is not consistent with our observation. Recall that all the experiments are performed in deionized water, so water diffusion should be suppressed except perhaps at the crack tip. Most importantly, we have carried out some experiments with the specimen immersed in mineral oil and observed the same behavior (see section SI 5). This suggested the role of water diffusion has no practical effect on our results.

Acknowledgments

This material is based upon work supported by the National Science Foundation under Grant No. CMMI-1903308. The authors supported by NSF are Hui, Zehnder Wang and Zhu. This research is partially supported by the Japan Society for the Promotion of Science KAKENHI grant no. JP17H06144 and JP22H04968 to Gong and grant no. JP19K23617 and JP21K14677 to Cui.

References

[1] J.P. Gong, Y. Katsuyama, T. Kurokawa, Y. Osada, Double-network hydrogels with extremely high mechanical strength, Adv. Mater. 15 (2003) 1155–1158. https://doi.org/10.1002/adma.200304907.

[2] J.Y. Sun, X. Zhao, W.R.K. Illeperuma, O. Chaudhuri, K.H. Oh, D.J. Mooney, J.J. Vlassak, Z. Suo, Highly stretchable and tough hydrogels, Nature. 489 (2012) 133–136. https://doi.org/10.1038/nature11409.

[3] R.J. Wojtecki, M.A. Meador, S.J. Rowan, Using the dynamic bond to access macroscopically responsive structurally dynamic polymers, Nat. Mater. 10 (2011) 14–27. https://doi.org/10.1038/nmat2891.

[4] Z. Wei, J.H. Yang, J. Zhou, F. Xu, M. Zrínyi, P.H. Dussault, Y. Osada, Y.M. Chen, Self-healing gels based on constitutional dynamic chemistry and their potential applications, Chem. Soc. Rev. 43 (2014) 8114–8131. https://doi.org/10.1039/c4cs00219a.

[5] D.L. Taylor, M. in het Panhuis, Self-Healing Hydrogels, Adv. Mater. 28 (2016) 9060–9093. https://doi.org/10.1002/adma.201601613.

[6] K. Yu, A. Xin, Q. Wang, Mechanics of self-healing polymer networks crosslinked by dynamic bonds, J. Mech. Phys. Solids. 121 (2018) 409–431. https://doi.org/10.1016/j.jmps.2018.08.007.

[7] Y.X. Lu, Z. Guan, Olefin metathesis for effective polymer healing via dynamic exchange of strong carbon-carbon double bonds, J. Am. Chem. Soc. 134 (2012) 14226–14231. https://doi.org/10.1021/ja306287s.

[8] C. Wang, N. Liu, R. Allen, J.B.H. Tok, Y. Wu, F. Zhang, Y. Chen, Z. Bao, A rapid and efficient self-healing thermo-reversible elastomer crosslinked with graphene oxide, Adv. Mater. 25 (2013) 5785–5790. https://doi.org/10.1002/adma.201302962.

[9] K. Mayumi, J. Guo, T. Narita, C.Y. Hui, C. Creton, Fracture of dual crosslink gels with permanent and transient crosslinks, Extreme Mech. Lett. 6 (2016) 52–59. https://doi.org/10.1016/j.eml.2015.12.002.

[10] C. Wang, H. Wu, Z. Chen, M.T. Mcdowell, Y. Cui, Z. Bao, Self-healing chemistry enables the stable operation of silicon microparticle anodes for high-energy lithium-ion batteries, Nat. Chem. 5 (2013) 1042–1048. https://doi.org/10.1038/nchem.1802.

[11] J. Liu, C.S.Y. Tan, Z. Yu, Y. Lan, C. Abell, O.A. Scherman, Biomimetic Supramolecular Polymer Networks Exhibiting both Toughness and Self-Recovery, Adv. Mater. 29 (2017). https://doi.org/10.1002/adma.201604951.

[12] T. Lin Sun, T. Kurokawa, S. Kuroda, A. bin Ihsan, T. Akasaki, K. Sato, M. Anamul Haque, T. Nakajima, J. Ping Gong, Physical hydrogels composed of polyampholytes demonstrate high toughness and viscoelasticity, Nat. Mater. 12 (2013). 932–937. https://doi.org/10.1038/NMAT3713.

[13] F. Luo, T.L. Sun, T. Nakajima, T. Kurokawa, Y. Zhao, K. Sato, A. bin Ihsan, X. Li, H. Guo, J.P. Gong, Oppositely charged polyelectrolytes form tough, self-healing, and rebuildable hydrogels, Adv. Mater. 27 (2015) 2722–2727. https://doi.org/10.1002/adma.201500140.

[14] N. Roy, B. Bruchmann, J.M. Lehn, DYNAMERS: Dynamic polymers as self-healing materials, Chem. Soc. Rev. 44 (2015) 3786–3807. https://doi.org/10.1039/c5cs00194c.

[15] T. Song, B. Jiang, Y. Li, Z. Ji, H. Zhou, D. Jiang, I. Seok, V. Murugadoss, N. Wen, H. Colorado, Self-healing Materials: A Review of Recent Developments, ES Mater. Manuf. (2021). https://doi.org/10.30919/esmm5f465.

[16] X. Li, K. Cui, T.L. Sun, L. Meng, C. Yu, L. Li, C. Creton, T. Kurokawa, J.P. Gong, Mesoscale bicontinuous networks in self-healing hydrogels delay fatigue fracture, Proc. Natl. Acad. Sci. U.S.A. 117 (2020) 7606–7612. https://doi.org/10.1073/PNAS.2000189117.

[17] J. Li, Z. Suo, J.J. Vlassak, Stiff, strong, and tough hydrogels with good chemical stability, J. Mater. Chem. B. 2 (2014) 6708–6713. https://doi.org/10.1039/c4tb01194e.

[18] J. Li, W.R.K. Illeperuma, Z. Suo, J.J. Vlassak, Hybrid hydrogels with extremely high stiffness and toughness, ACS Macro Lett. 3 (2014) 520–523. https://doi.org/10.1021/mz5002355.

[19] J. Guo, A.T. Zehnder, C. Creton, C.Y. Hui, Time dependent fracture of soft materials: Linear: versus nonlinear viscoelasticity, Soft Matter. 16 (2020) 6163–6179. https://doi.org/10.1039/d0sm00097c.

[20] C.-Y. Hui, F. Cui, A. Zehnder, F.J. Vernerey, Physically motivated models of polymer networks with dynamic cross-links: comparative study and future outlook, Proc. R. Soc. London, Ser. A. 477 (2021). https://doi.org/10.1098/rspa.2021.0608.

[21] G.I. Bell, Models for the specific adhesion of cells to cells, Science (1979). 200 (1978) 618–627. https://doi.org/10.1126/science.347575.

[22] K. Kothari, Y. Hu, S. Gupta, A. Elbanna, Mechanical Response of Two-Dimensional Polymer Networks: Role of Topology, Rate Dependence, and Damage Accumulation, ASME J. Appl. Mech. 85 (2018). https://doi.org/10.1115/1.4038883.

[23] S.C. Lamont, J. Mulderrig, N. Bouklas, F.J. Vernerey, Rate-Dependent Damage Mechanics of Polymer Networks with Reversible Bonds, Macromolecules. 54 (2021) 10801–10813. https://doi.org/10.1021/acs.macromol.1c01943.

[24] A. Ghareeb, A. Elbanna, Modeling fracture in rate-dependent polymer networks: A quasicontinuum approach, ASME J. Appl. Mech. 88 (2021). https://doi.org/10.1115/1.4051658.

[25] F.J. Vernerey, Mechanics of transient semi-flexible networks: Soft-elasticity, stress relaxation and remodeling, J. Mech. Phys. Solids. 160 (2022). https://doi.org/10.1016/j.jmps.2022.104776.

[26] T.L. Sun, T. Kurokawa, S. Kuroda, A. bin Ihsan, T. Akasaki, K. Sato, M.A. Haque, T. Nakajima, J.P. Gong, Physical hydrogels composed of polyampholytes demonstrate high toughness and viscoelasticity, Nat. Mater. 12 (2013) 932–937. https://doi.org/10.1038/nmat3713.

[27] M. Liu, J. Guo, C.Y. Hui, A.T. Zehnder, Application of Digital Image Correlation (DIC) to the Measurement of Strain Concentration of a PVA Dual-Crosslink Hydrogel Under

Large Deformation, Exp. Mech. 59 (2019) 1021–1032. https://doi.org/10.1007/S11340-019-00520-4.

[28] K.J. Henderson, T.C. Zhou, K.J. Otim, K.R. Shull, Ionically cross-linked triblock copolymer hydrogels with high strength, Macromolecules. 43 (2010) 6193–6201. https://doi.org/10.1021/MA100963M.

[29] T. Narita, K. Mayumi, G. Ducouret, P. Hébraudhébraud, Viscoelastic Properties of Poly(vinyl alcohol) Hydrogels Having Permanent and Transient Cross-Links Studied by Microrheology, Classical Rheometry, and Dynamic Light Scattering, Macromolecules. 46 (2013) 4174–4183. https://doi.org/10.1021/ma400600f.

[30] Z. Zhang, Q. Chen, R.H. Colby, Dynamics of associative polymers, Soft Matter. 14 (2018) 2961–2977. https://doi.org/10.1039/C8SM00044A.

[31] K. Cui, Y.N. Ye, T.L. Sun, C. Yu, X. Li, T. Kurokawa, J.P. Gong, Phase separation behavior in tough and self-healing polyampholyte hydrogels, Macromolecules, 53 (2020) 5116–5126. https://doi.org/10.1021/acs.macromol.0c00577

Supplementary Information for

Load transfer between permanent and dynamic networks due to stress gradients in nonlinear viscoelastic hydrogels

Jikun Wang[1], Kunpeng Cui[2,5], Bangguo Zhu[1], Jian Ping Gong[2,3,4,*], Chung-Yuen Hui[1,3,*] and Alan T. Zehnder[1,*]

*Corresponding author:
Jian Ping Gong[2,3,4,*], Chung-Yuen Hui[1,3,*] and Alan Zehnder[1,*]

Email: gong@sci.hokudai.ac.jp, ch45@cornell.edu, atz2@cornell.edu

Table of Contents

S1. Supplementary Methods

Digital Image correlation (DIC) for PA tension tests. We use the Ncorr module in MATLAB [1] to analyze DIC data. In Ncorr, the reference image can be updated based on the correlation coefficient, so it can measure large deformation precisely. Details of the DIC procedure are given in our previous works [2,3]. Briefly, we used airbrush to create random speckle patterns on the surface of PA gel. Photographs of these samples were taken 5 times per second during tests. The photos for DIC measurements were acquired using a charged-coupled device (CCD) camera (FLIR Grasshop-per3 4.1 MP mono) with a telecentric lens (Edmund Optics, SilverTL 0.16x). Selected pictures were imported into MATLAB and the strain fields were calculated using Ncorr.

Large strain analysis is activated in Ncorr to update the reference image. The important input parameters are the subset radius, the radius of a circular subset used to correlate sub-images, is set to 20; the subset spacing, the spacing between neighboring subsets, is set to 2; and the strain radius, the size of the region over which displacement data are fitted to a plane to calculate the displacement gradient, is set to 5. The choice of these parameters is determined by the quality of speckle patterns and the strain distribution and may vary from test to test.

Uniaxial tension tests. We use uniaxial tension tests to determine the parameters for our PA models in Eqns. (S4a-c) and (S5a-c) below. These tests are conducted on rectangular PA gel specimens of dimension 30mm (length) x 10mm (width) x 2mm (thickness), as shown in Figure S1. Three cyclic tests and one relaxation test are carried out to determine the parameters for the p-PA and c-PA gels. For cyclic tests, we stretch the sample to a stretch ratio of 3 with stretch rate 1/s, 0.1/s and 0.01/s respectively and then unload them

to their original lengths (stretch ratio = 1) at the same rates. For the relaxation test, we stretch the sample to a stretch ratio of 3 with stretch rate 0.5/s and then hold for a half hour. All tests are done in deionized water to prevent the gels from drying.

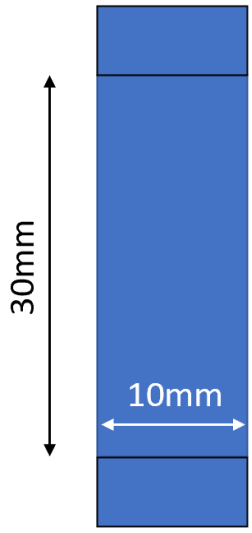

Fig. S1 Schematic of uniaxial tension specimen to determine material parameters for constitutive models

S2. Review of viscoelastic models for PA gels

In this section we summarize our model which describes the constitutive behavior of PA gels. Since this model has been studied in detail in our previous works [4,5], we list equations that are relevant to this work and focus on explaining the physics in the model. Readers who are interested in the connection of this model with statistical mechanics approach are encouraged to read our recent work [6].

c-PA gel model

Let us start with the c-PA gel and consider uniaxial tension. In our model, the 1st Piola or nominal stress *P(t)* is the sum of the stress acting on the permanent network and the stress supported by the dynamic network. The stress acting on the permanent network depends only on the *current* deformation gradient and is given by:

$$\omega_{\text{chem}} \times 2 \left. \frac{dW_0}{dI_1} \right|_{I_1(t)} \left(\lambda(t) - \lambda(t)^{-2} \right) \tag{S1}$$

where ω_{chem} is the molar fraction of chemical crosslinks per unit undeformed volume and W_0 is the strain energy density function for the chemical network. Since the gel is incompressible, we assume W_0 depends only on the invariant of the right Cauchy-Green tensor $I_1(t) = \text{trace}\left[\left(\mathbf{F}^{0\to t} \right)^T \left(\mathbf{F}^{0\to t} \right) \right]$, where $\mathbf{F}$ is the deformation gradient tensor. The superscript $0 \to t$ in the deformation gradient tensor $\mathbf{F}^{0\to t}$ indicates that it is measured from the reference configuration at $t = 0$ when the gel is undeformed. In uniaxial loading, $I_1(t) = \lambda^2(t) + \frac{2}{\lambda(t)}$, where λ is the stretch ratio in the tensile test. Hence eq. (S1) is a direct consequence of hyper-elasticity.

Unlike the chemical cross-links in the permanent network, crosslinks formed from physical bonds in the dynamic network can break and heal. We assume that before loading ($t < 0$), the physical crosslinks have reached a state of dynamic equilibrium in which the healing rate is equal to the breaking rate; this steady state healing rate is denoted by χ^{ss} . However, once loading starts (at $t > 0$), the physical bonds can break and heal at different rates. In our model, it is assumed that when a physical bond breaks, it completely unloads and loses all its strain energy. Therefore a newly reformed crosslink at time τ has zero initial energy and the stress carried by it at current time $t > \tau$ depends on $H^{\tau\to t} \equiv \text{trace}\left[\left(\mathbf{F}^{\tau\to t}\right)^T \mathbf{F}^{\tau\to t}\right]$, where the superscript $\tau \to t$ in the deformation gradient tensor $\mathbf{F}^{\tau\to t}$ indicates that deformation is measured with respect to the configuration at τ. For uniaxial tension, $H^{\tau\to t} = \frac{\lambda(t)}{\lambda^2(\tau)} - \frac{\lambda(\tau)}{\lambda^2(t)}$. Note that $H^{t\to t} = 0$, consistent with the fact that physical crosslinks carry no load at birth.

Next, we determine the stress carried by the dynamic network at current time *t*. Let $\chi(\tau)$ denote the healing rate at time τ, where $0 \le \tau < t$. More precisely, the molar fraction of chains per unit reference volume that are born between $\tau, \tau + d\tau$ is $\chi(\tau)d\tau$. Let $\phi_B(\tau, t, H^{\tau\to t})$ denote the survivability function which is the fraction of physical bonds *that survive from the time of their birth at time* τ *to the current time* t. This fraction is equal to 1 at $t = \tau$ and goes to zero for $t >> \tau$. The nominal stress carried by this subpopulation of the chains is

$$\left[\chi(\tau)d\tau\right] \times \phi\left(\tau, t, H^{\tau\to t}\right) \times 2\frac{dW_0}{dI_1}\bigg|_{I_1 = H^{\tau\to t}} \left[\frac{\lambda(t)}{\lambda^2(\tau)} - \frac{\lambda(\tau)}{\lambda^2(t)}\right] \qquad \text{(S2a)}$$

The stress carried by the bonds that heal or reform for time $t > 0$ (after loading) is obtained by summing the contribution of the stress carried by all subpopulations. This is done by integrating over τ, i.e.,

$$\int_0^t \chi(\tau)\times\phi\left(\tau,t,H^{\tau\to t}\right)\times 2\frac{dW_0}{dI_1}\bigg|_{I_1=H^{\tau\to t}}\left[\frac{\lambda(t)}{\lambda^2(\tau)}-\frac{\lambda(\tau)}{\lambda^2(t)}\right]d\tau \tag{S2b}$$

To this eq. (S2b) we must add the stress carried by the physical bonds that are connected and survive to the current time t before loading, which is

$$2\rho\phi_B(\tau=0,t,H^{0\to t})\frac{dW_0}{dI_1}\bigg|_{I_1(t)}\left(\lambda(t)-\lambda(t)^{-2}\right), \tag{S3}$$

where ρ is the molar fraction of connected physical cross-links before the start of loading. The nominal stress is the sum of eq. (S1), eq. (S2b) and eq. (S3), i.e.,

$$\begin{aligned}P(t)=\omega_{\text{chem}}\times 2\frac{dW_0}{dI_1}\bigg|_{I_1(t)}\left(\lambda(t)-\lambda(t)^{-2}\right)+2\rho\frac{dW_0}{dI_1}\bigg|_{I_1(t)}\phi_B(\tau=0,t,H^{0\to t})\left(\lambda(t)-\lambda(t)^{-2}\right)\\ +\int_0^t\left[\chi(\tau)\phi_B\left(\tau,t,H^{\tau\to t}\right)2\frac{dW_0}{dI_1}\bigg|_{I_1=H^{\tau\to t}}\left[\frac{\lambda(t)}{\lambda^2(\tau)}-\frac{\lambda(\tau)}{\lambda^2(t)}\right]\right]d\tau,\end{aligned} \tag{S4a}$$

In previous works [4] we have proposed that the survivability function $\phi_B(\tau,t,H^{\tau\to t})$ has the form:

$$\phi_B(\tau,t,H^{\tau\to t})=\left[1+\frac{\alpha_B-1}{t_B}\int_\tau^t f\left(H^{\tau\to s}\right)ds\right]^{\frac{1}{1-\alpha_B}}. \tag{S4b}$$

In eq. (S4b), t_B is the characteristic breaking time of physical bonds, $\alpha_B \in (1, 2)$ is a material parameter that controls the rate of decay of the survivability function and f is a

function which measures the dependence of breaking rate on the stretch experienced by a physical cross-link from its formation at time τ to the current time $t > \tau$ [4]. It is given by

$$f\left(H^{\tau\to s}\right) = \exp\left\{\left(1+\frac{H^{\tau\to s}-3}{I_c-3}\right)^m - 1\right\} \tag{S4c}$$

where I_c is the first invariant of the right Cauchy-Green tensor calculated at the critical stretch λ_c in a tension test, after which the bond breaking kinetics accelerate, and m is a material parameter. Equation (S4c) expresses the fact that when chains stretch beyond their critical strain limit, their breaking rate increase significantly resulting in macroscopic softening of the gel. For a *linear viscoelastic* solid, *f* is the constant function *1* $\left(I_c \to \infty\right)$ so that the survivability function in eq. (S4b) is independent of strain history [7,8].

To complete the model, one needs to supply the healing rate $\chi(t)$ in eq. (S4a). In our previous works [4,5], we have shown that the healing rate depends on the deformation history and is obtained by solving the integral equation:

$$1-\omega_{\text{chem}} = \chi(t)t_H + \int_{-\infty}^{t} \phi_B(\tau,t,H^{\tau\to t})\chi(\tau)d\tau, \tag{S4d}$$

where t_H is the characteristic time for healing.

p-PA gel model

The model for p-PA gel is almost identical, except that there is no permanent network. This permanent network is replaced by a second dynamic network is added to account for the presence of two phases [5].

With this modification, eq. (S4a) becomes

$$P(t) = \left[\sum_{i=1}^{2} \chi_i^{ss} \frac{t_{Bi}}{2-\alpha_{Bi}} [\phi_{Bi}(\tau = 0, t, H^{0\to t})]^{2-\alpha_{Bi}}\right] \times 2 \frac{dW_0}{dI_1}\Big|_{I_1(t)} (\lambda(t) - \lambda(t)^{-2}) +$$

$$\sum_{i=1}^{2} \int_0^t \left[\chi_i(\tau)\phi_{Bi}(\tau, t, H^{\tau\to t}) \times 2 \frac{dW_0}{dI_1}\Big|_{H^{\tau\to t}} \left[\frac{\lambda(t)}{\lambda^2(\tau)} - \frac{\lambda(\tau)}{\lambda^2(t)}\right]\right] d\tau \qquad \text{(S5a)}$$

The summation indices $i = 1,2$ specify the two phases, each has its material parameters, (χ_i^{ss}, t_{Bi}, α_{Bi}, etc.,) , healing rate χ_i and survivability function $\phi_{Bi}(\tau, t, H^{\tau\to t})$. The healing rate of each phase is determined by the integral equation:

$$\omega_i = \chi_i(t) t_{H_i} + \int_{-\infty}^{t} \phi_{B_i}(\tau, t) \chi_i(\tau) d\tau \qquad i=1,2 \qquad \text{(S5b)}$$

where $\omega_1, \omega_2 = 1 - \omega_1$ are the molar fraction of weak and strong bonds in the hard and soft phase respectively.

S3. Determination of model parameters

We used two methods to determine the parameters for the constitutive models for the p-PA and c-PA gels. In both methods, we first define a parameter space for the fitting. The parameter space for the p-PA model is

$C1 \in [0, 5] \quad C2 \in [0, 0.3] \quad C3 \in [0, 0.1] \quad \lambda_c \in [1.05, 1.3]$

$w_1 \in [0.3, 0.7] \quad \alpha_{B1} \in [1.3, 1.9] \quad t_{B1} \in [0, 0.02] \quad m_1 \in [0.3, 0.7] \quad t_{H1} \in [0, 1]$

$w_2 \in [0.3, 0,7] \quad \alpha_{B2} \in [1.3, 1.9] \quad t_{B2} \in [0, 0.2] \quad m_2 \in [0.3, 0.7] \quad t_{H2} \in [0, 1]$

The parameter space for c-PA model is

$C1 \in [0, 5] \quad C2 \in [0, 0.3] \quad C3 \in [0, 0.1] \quad \lambda_c \in [1.05, 3.00] \quad w_{chem} \in [0, 0.15]$

$\alpha_B \in [1.3, 1.9] \quad t_B \in [0, 0.2] \quad m \in [0.3, 0.7] \quad t_H \in [0, 1]$

where $C1, C2, C3$ define the Yeoh's strain energy W_0 in Eqn. (S4a) or (S5a), that is,

$$W_0(I_1) = C1(I_1 - 3) + C1C2(I_1 - 3)^2 + C1C3(I_1 - 3)^3 \qquad \text{(S6)}$$

Specifically, $\mu = 2C1$ is small strain shear modulus of the undamaged PA gel, C1 and C2 controls the strain stiffening characteristic of the network. The fitting results for different PA gels are shown in Table S1-S4.

***Method I*: Large dataset computing**

We randomly pick 1 million sets of parameters from the parameter space and calculate the nominal stress using the constitutive model for each test 1 million times based on these 1 million sets of parameters. Using mean square error as criteria, we pick one set of parameters out of these 1 million sets of parameters which fit our experimental data best. The optimal parameters for p-PA and c-PA are shown in Table S1 and S2 respectively. From Figures S2 – S5 we find that the fitting results are good. However, this method takes us several hours to finish even with a powerful workstation.

***Method 2*: Machine learning**

To make the fitting process more scalable, we also developed a machine learning method to determine the parameters. Details of this method can be found in our previous paper [9]. Briefly, we randomly pick 3000 sets of parameters instead of 1 million from the parameter set and then use our model to compute the nominal stress history 3000 times for each test. Then we use machine learning to build metamodels for PA constitutive models based on these 3000 cases. After learning, we use the metamodels to predict the results of constitutive models on 1 million sets of parameters without really computing the constitutive models 1 million times. This method can be implemented in a laptop (CPU – Intel i7-9750H, 4 cores, GPU – Nvidia GTX 1650) in a half hour and the fitting results are just as good as those shown in Figures S2 and S5.

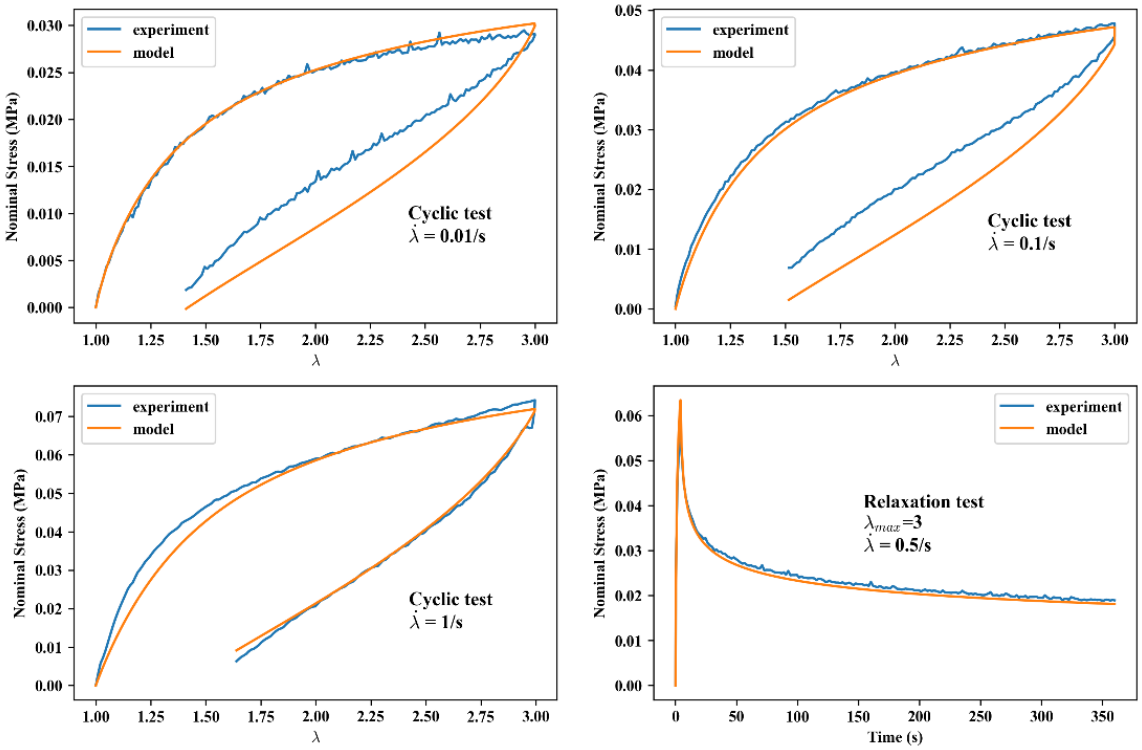

Fig. S2. Fitting results for *p-PA*$_{weak}$. In cyclic test the loading and unloading rates have the same magnitude. In relaxation tests, we first stretch the sample at a rate of 0.5s, then held the stretch ratio constant when it reaches 3.

Table S1. Fitting parameters for *p-PA*$_{weak}$

$C_1 = 0.1000MPa$	$C_2 = 0.0500$	$C_3 = 0.0000$	$\lambda_c = 1.2600$	
$\omega_1 = 0.5729$	$\alpha_{B1} = 1.7448$	$t_{B1} = 0.0058$	$m1 = 0.3635$	$t_{H1} = 0.5301$
$\omega_2 = 0.4271$	$\alpha_{B2} = 1.8404$	$t_{B2} = 0.1529$	$m2 = 0.5277$	$t_{H2} = 0.7351$

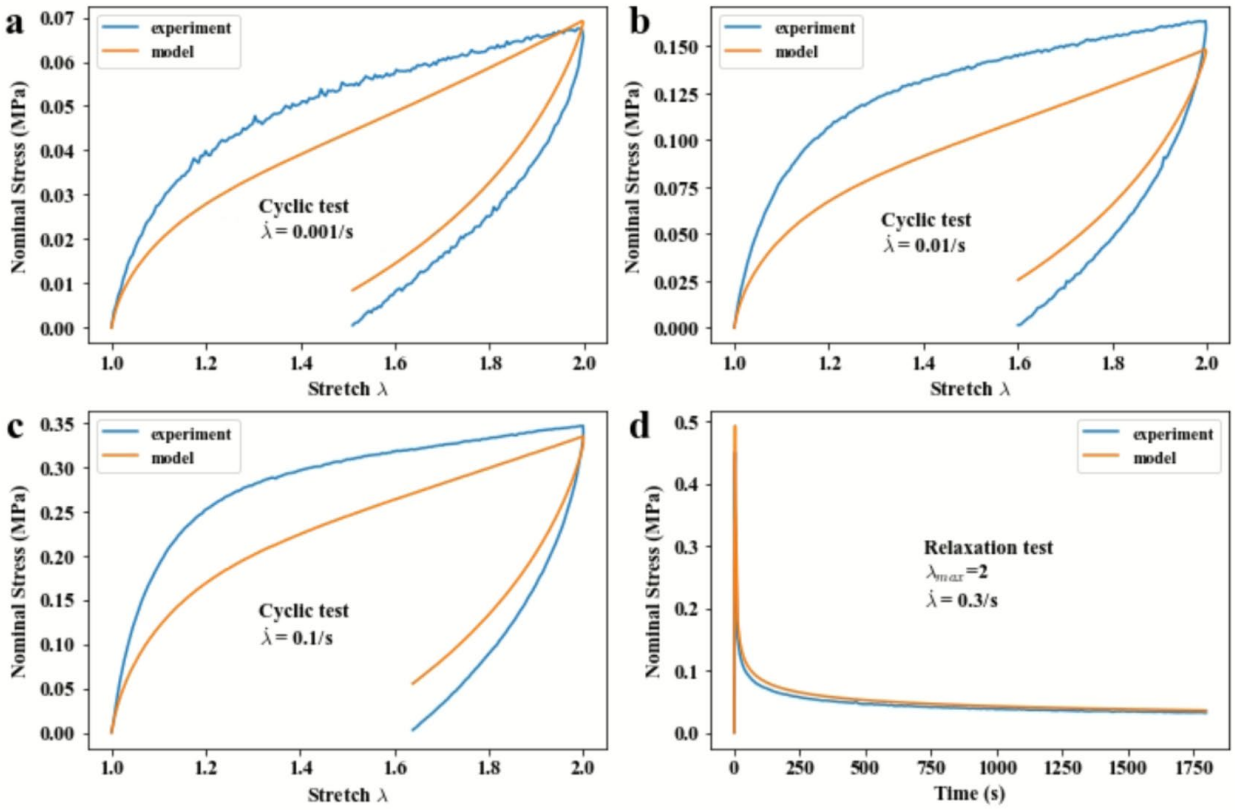

Fig. S3. Fitting results for *p-PA*$_{strong}$. In cyclic test the loading and unloading rates have the same magnitude. In relaxation tests, we first stretch the sample at a rate of 0.3s, then held the stretch ratio constant when it reaches 2.

Table S2. Fitting parameters for *p-PA*$_{strong}$

$C_1 = 3.990MPa$	$C_2 = 0.506000$	$C_3 = 0.0352$	$\lambda_c = 1.1560$	
$\omega_1 = 0.7500$	$\alpha_{B1} = 1.7957$	$t_{B1} = 0.0051$	$m1 = 0.4375$	$t_{H1} = 0.4289$
$\omega_2 = 0.2500$	$\alpha_{B2} = 1.6938$	$t_{B2} = 0.0183$	$m2 = 0.4831$	$t_{H2} = 0.0940$

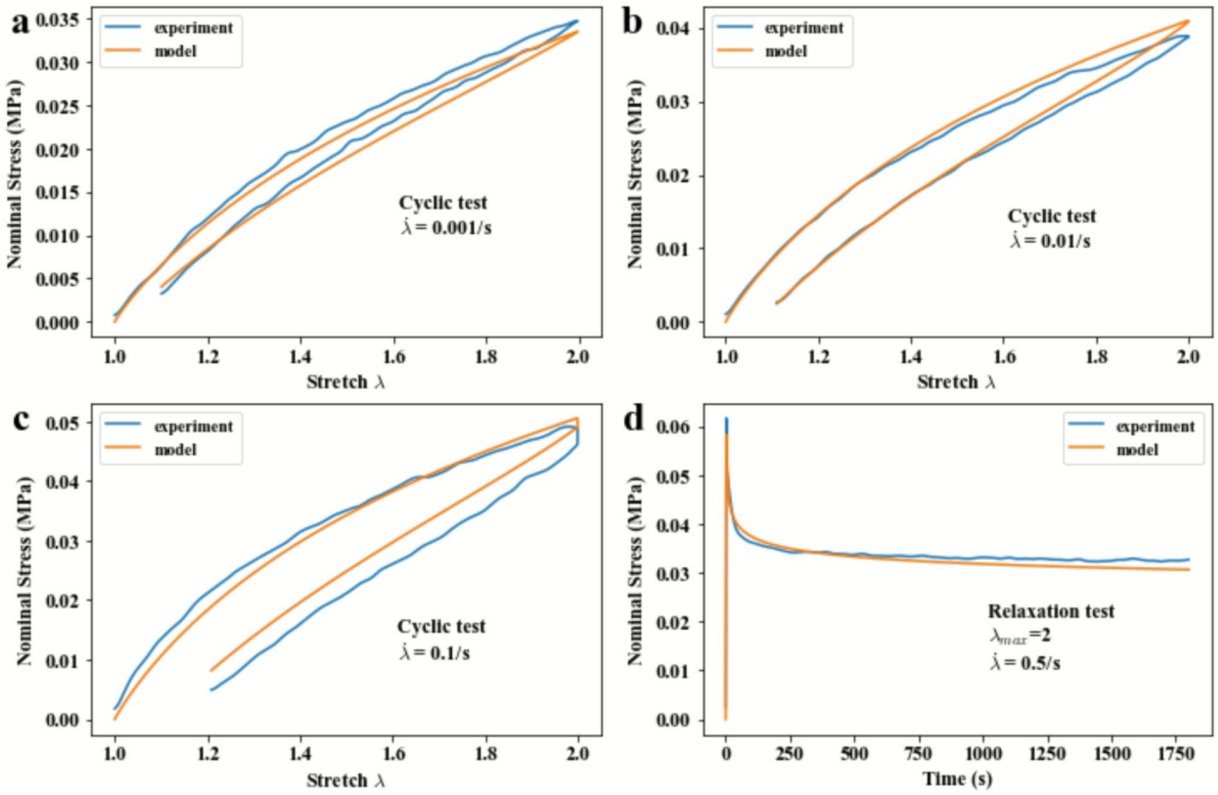

Fig. S4. Fitting results for *c-PA*$_{weak}$. In cyclic test the loading and unloading rates have the same magnitude. In relaxation tests, we first stretch the sample at a rate of 0.5s, then held the stretch ratio constant when it reaches 2.

Table S3. Fitting parameters for *c-PA*$_{weak}$

$C_1 = 0.05682MPa$	$C_2 = 0.0011$	$C_3 = 0.0000$	$\lambda_c = 2.565$	
$\omega_{chem} = 0.0898$	$\alpha_B = 1.8717$	$t_B = 0.0612$	$m = 1.8017$	$t_H = 0.8021$

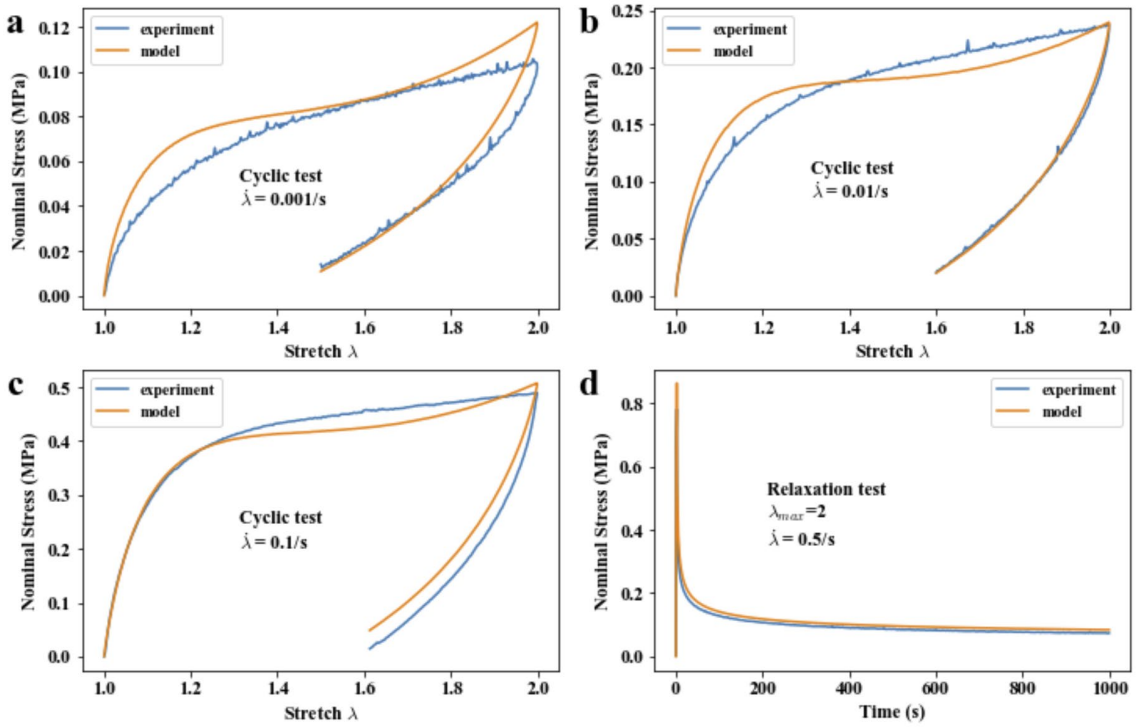

Fig. S5. Fitting results for *c-PA*$_{strong}$. In cyclic test the loading and unloading rates have the same magnitude. In relaxation tests, we first stretch the sample at a rate of 0.5s, then held the stretch ratio constant when it reaches 2.

Table S4. Fitting parameters for *c-PA*$_{strong}$

$C_1 = 2.3416MPa$	$C_2 = 0.1147$	$C_3 = 0.0535$	$\lambda_c = 1.0550$	
$\omega_{chem} = 0.0026$	$\alpha_B = 1.7190$	$t_B = 0.0718$	$m = 0.3079$	$t_H = 0.312$

S4. Model simulation of T-shape specimen test

To simulate the relaxation process, we use eqn. (S4a-d) and eqn. (S5a-b). In our relaxation experiments, the stretch history λ_N at the grip is known, i.e.,

$$\lambda_N(t) = \begin{cases} 1 + 0.1 \times t & 5s > t > 0 \\ 1.5 & t \geq 5s \end{cases} \tag{S7}$$

We assume that the 1st Piola or nominal stress and stretch in each section are uniform and denote them by $P_{ns}, P_{ws}, \lambda_{ns}, \lambda_{ws}$ respectively. Our assumption implies that

$$\lambda_N = \frac{\lambda_{ns} + \lambda_{ws}}{2} \tag{S8}$$

Force balance implies that

$$P_{ns} A_{ns} = P_{ws} A_{ws} = F \tag{S9}$$

where A_{ns}, A_{ws} denote the cross-section area of the specimen in the undeformed state and F is the force acting on the specimen. Equations (S4a-d), (S6-8) allow us to numerically determine the time evolution of stretch ratios $\lambda_{ns}, \lambda_{ws}$ for the c-PA gel. The same procedure, with eq. (S4a-d) replaced by eq. (S5a-b), determines $\lambda_{ns}, \lambda_{ws}$ for the p-PA gel. The numerical algorithm to determine the stress history is based on the fact that the force acting on the two sections is the same. In each timestep, we first guess the length of two sections with the constraint that the sum of their length is equal to the overall length which at each time step is a constant. Then we use our constitutive model e.g., (S4a-d) to calculate the nominal stress on each section at this timestep. The force acting on each section is obtained using these nominal stresses. If the difference between these forces are less than 1Pa, we adopt these lengths and go to next timestep. If not, we re-estimate the length of

two parts according to the difference between the force of two parts. The flow chart of our numerical scheme is shown in Figure S6.

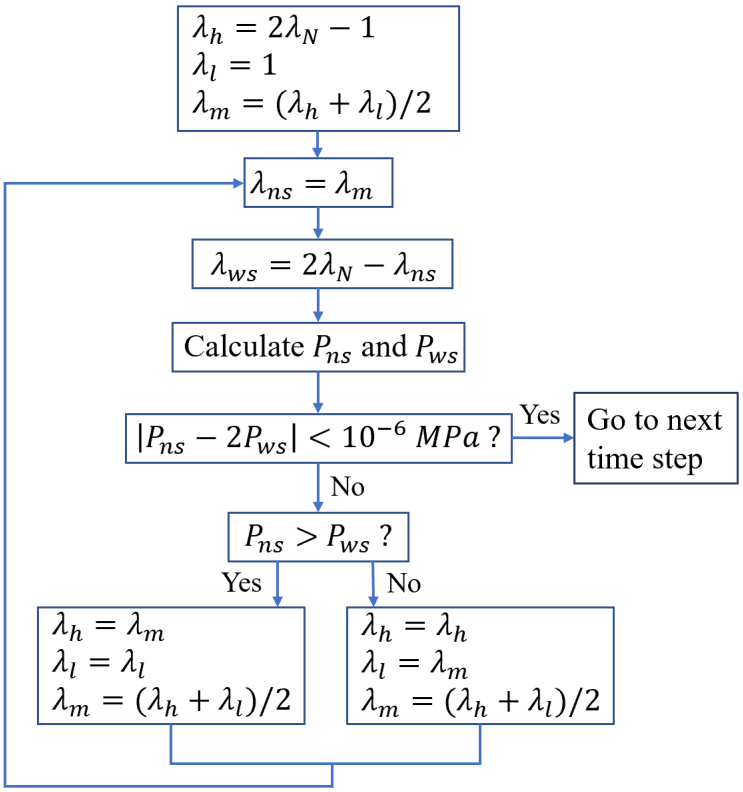

Fig. S6. Flow chart for calculating stretches of T-shape sample in each time step. The subscripts ns and ws denote narrow and wide section respectively. λ_N is the nominal stretch imposed on the specimen. $\lambda_h, \lambda_l, \lambda_m$ are intermediate variables in this algorithm to store relevant stretches.

S5. Relaxation test for T-shape sample in oil

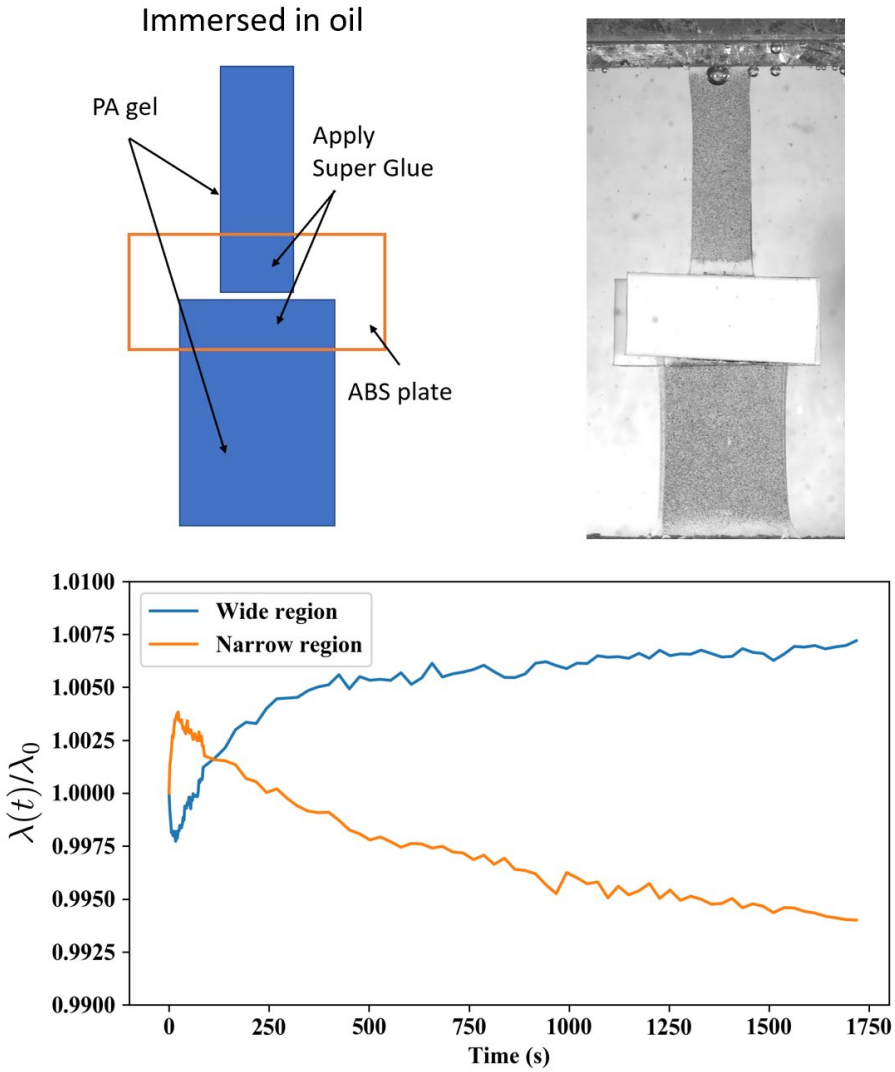

Fig. S6. T-shape test for *c-PA*$_{strong}$ immersed in mineral oil.

The sample is made of two separated parts so there is no water flow within this sample. The sample is stretched to $\lambda_N = L/L_0 = 1.3$ with a fast stretch rate of 0.1/s and then hold it at the deformed length $L = 1.3L_0$ for half an hour. The curves show the time evolution of stretch at narrow and wide sections, which have the same trend as the curve of T-shape test in water.

SI References

[1] J. Blaber, B. Adair, A. Antoniou, Ncorr: Open-Source 2D Digital Image Correlation Matlab Software, https://doi.org/10.1007/s11340-015-0009-1.

[2] M. Liu, J. Guo, C.Y. Hui, A.T. Zehnder, Application of Digital Image Correlation (DIC) to the Measurement of Strain Concentration of a PVA Dual-Crosslink Hydrogel Under Large Deformation, Exp. Mech. 59 (2019) 1021–1032. https://doi.org/10.1007/S11340-019-00520-4.

[3] M. Liu, J. Guo, Z. Li, C.Y. Hui, A.T. Zehnder, Crack propagation in a PVA dual-crosslink hydrogel: Crack tip fields measured using digital image correlation, Mech. Mater. 138 (2019) 103158. https://doi.org/10.1016/J.MECHMAT.2019.103158.

[4] S. P. Venkata, K. Cui, J. Guo, A.T. Zehnder, J.P. Gong, C.Y. Hui, Constitutive modeling of strain-dependent bond breaking and healing kinetics of chemical polyampholyte (PA) gel, Soft Matter. 17 (2021) 4161–4169. https://doi.org/10.1039/D1SM00110H.

[5] S. P. Venkata, K. Cui, J. Guo, A.T. Zehnder, J.P. Gong, C.Y. Hui, Constitutive modeling of bond breaking and healing kinetics of physical Polyampholyte (PA) gel, Extreme Mech. Lett. 43 (2021) 101184. https://doi.org/10.1016/j.eml.2021.101184.

[6] C.Y. Hui, F. Cui, A. Zehnder, F.J. Vernerey, Physically motivated models of polymer networks with dynamic cross-links: comparative study and future outlook, Proc. R. Soc. London, Ser. A. 477 (2021). https://doi.org/10.1098/rspa.2021.0608.

[7] R. Long, K. Mayumi, C. Creton, T. Narita, C.Y. Hui, Rheology of a dual crosslink self-healing gel: Theory and measurement using parallel-plate torsional rheometry, J. Rheol. 59 (2015) 643. https://doi.org/10.1122/1.4915275.

[8] J. Guo, R. Long, K. Mayumi, C.Y. Hui, Mechanics of a Dual Cross-Link Gel with Dynamic Bonds: Steady State Kinetics and Large Deformation Effects, Macromolecules. 49 (2016) 3497–3507. https://doi.org/10.1021/acs.macromol.6b00421

[9] J. Wang, T. Li, F. Cui, C.Y. Hui, J. Yeo, A.T. Zehnder, Metamodeling of constitutive model using Gaussian process machine learning, J. Mech. Phys. Solids. 154 (2021) 104532. https://doi.org/10.1016/J.JMPS.2021.104532.